Two-color resonant filamentation in gases

J. Doussot, P. Béjot,* and O. Faucher
Laboratoire Interdisciplinaire CARNOT de Bourgogne, UMR 6303 CNRS-Université Bourgogne Franche-Comté, 9 Av. A. Savary, BP 47870, F-21078 DIJON Cedex, France
(Received 4 April 2016; published 5 July 2016)

In this paper, it is shown that two-photon resonance involving a fundamental field and one of its odd harmonic strongly influences the filamentation process, i.e., the nonlinear propagation of an ultrashort and ultraintense laser field. This particular situation happens, for instance, when a 400 nm fundamental field propagates together with its third harmonic in krypton. Using three-dimensional *ab initio* calculations, the optical response of krypton is evaluated and the underlying nonlinear refractive indices are extracted. It is found that the resonance also exacerbates higher-order nonlinear processes. Injecting the retrieved higher-order Kerr indices in a nonlinear propagation solver, it is found that the resonance leads to an enhanced defocusing cross-phase modulation that strongly participates to the filament stabilization. This work sheds a light on the mechanism of filamentation, in particular, in the ultraviolet range, where two-color two-photon resonances are expected to occur in many atomic gases.

DOI: 10.1103/PhysRevA.94.013805

I. INTRODUCTION

Since its very first observation [1], laser filamentation in gases has been the subject of numerous theoretical and experimental studies. Induced by the dynamic equilibrium between different nonlinear effects, a filament can sustain very high intensities over very long distances, contrary to a laser pulse propagating linearly. The competition between the Kerr effect, responsible for beam self-focusing and plasma generation (i.e., ionization), responsible for beam defocusing, was rapidly identified as the underlying basic mechanism driving this self-guiding process. Nevertheless, a few years ago, time-resolved nonlinear refractive index measurements performed in gases seemed to show that Kerr effect saturates by itself and becomes a defocusing effect as the intensity increases [2]. This unexpected observation, called higher-order Kerr effect (HOKE), has raised an active debate about its interpretation and its possible impact on the filamentation process [3–16].

In this theoretical study, we exhibit a mechanism leading to HOKE in the case where a two-photon transition, involving a fundamental field and one of its odd harmonic, is close to an atomic resonance. In this situation, the cross-phase modulation induced by the generated odd harmonic on the fundamental is strongly enhanced, almost instantaneous, at least for a pulse duration higher than 10 fs, and leads to an inversion of the refractive index experienced by the fundamental field. Note that apart from this large negative cross-phase modulation, the presence of an odd harmonic also leads to a strong modification of ionization, a mechanism already reported in [17–20]. It is also shown that higher-order Kerr effect also impacts the process of odd-harmonic generation. Comparing the nonlinear polarization obtained by means of *ab initio* quantum calculations with a weak-field Taylor expansion of the field in the case of krypton for a 400 nm fundamental field accompanied with its third-harmonic, nonlinear susceptibilities are evaluated up to the eleventh order. Since the process takes place close to a resonance, the susceptibilities are highly frequency dependent, so that the nonlinear refractive indices responsible for self-, cross-phase modulation, third-harmonic generation, and three-photon generation (fission of a third-harmonic photon into three fundamental photons) have amplitudes that deviate by about two order of magnitudes and have different signs. Finally, using the fitted nonlinear refractive indices in a propagation code, it is shown that the above mentioned HOKE deeply impacts the filamentation dynamics and actively participates in the intensity clamping occurring during the filamentation process.

II. STRONG-FIELD EVALUATION OF ATOMIC OPTICAL RESPONSE

Close to a two-photon resonance, it is well known that the third-order nonlinear susceptibility is highly frequency dependent and can even become negative. For instance, it has been shown that the third-order nonlinear susceptibility responsible for self-phase modulation (SPM) in xenon becomes negative in the ultraviolet spectral region [21]. Here, we consider a completely different case in which the SPM lies far from any two-photon resonance (i.e., the third-order nonlinear susceptibility responsible for SPM is positive and leads to self-focusing), while the medium becomes defocusing because of a higher-order Kerr effect. The process described here takes place because, first, odd-harmonic generation occurs and, second, because there is a two-photon two-color atomic resonance leading to large negative cross-phase modulation (XPM) of the odd-harmonic pulse on the fundamental one. This particular situation happens, for instance, when a 400 nm fundamental field propagates in krypton. In this case, the simultaneous absorption of a fundamental and a third-harmonic photon (previously produced by third-harmonic generation) is close to resonance with both the $4p$-$5p$ ($\simeq$11.5 eV) and the $4p$-$6p$ ($\simeq$12.8 eV) two-photon transitions. In order to evaluate the optical response of the krypton atom when irradiated by a $\lambda_0 = 400$ nm field and its third harmonic, *ab initio* calculations have been performed under the single

*pierre.bejot@u-bourgogne.fr

active electron approximation. Technical details about the numerical method can be found in [13,22]. Briefly, the method consists in evaluating the time evolution of the electronic wave function $|\Psi\rangle$ when it is submitted to the influence of the atomic potential and a linearly polarized (along a direction denoted hereafter Z) electric field $E(t)$ by solving the time-dependent Schrödinger equation. The atomic potential used for representing krypton has been published recently [23]. The polarization P along Z is then calculated all along the interaction as $\langle\Psi|Z|\Psi\rangle$. The fundamental and third-harmonic (TH) fields considered during the calculations have a 14 fs (full width at half maximum) and 8 fs Gaussian temporal envelope profile, respectively. For the sake of clarity, only the complex envelopes of the nonlinear polarizations $\mathcal{P}_{\omega_0}(t)$ and $\mathcal{P}_{3\omega_0}(t)$ oscillating respectively around the fundamental frequency ω_0 and around the third-harmonic one are presented. They are obtained by an appropriate spectral filtering of the polarization and by removing the fast oscillating carrier field in the temporal domain. Following this procedure, the real (imaginary) part of the nonlinear polarization corresponds to the part that is in phase (out of phase) with the fundamental pulse. While *ab initio* calculations supply a very accurate description of the atom-field interaction, so far they require too high resources for numerical simulation propagation over macroscopic distances. Recent theoretical work has also developed an original approach describing analytically nonlinear optical processes in the strong-field regime [24]. This work allows one to evaluate in a more efficient way the optical response of an atom in the strong regime even in the case of a multicolor field but works well far from any atomic resonances, which is not the case here. The standard treatment in propagation simulations consists in approximating the optical response of the atom with a perturbation model, in which the atomic polarization is developed as a Taylor series of the field. Following this approach, it is found that the complex envelopes of the nonlinear polarizations derived from TDSE are well reproduced both in *shape and amplitude* by the following weak-field developments:

$$\mathcal{P}_{\omega_0}(t) = 2\sqrt{\frac{2\epsilon_0}{c}}\left(\sum_{l=1}^{2}\sum_{k=0}^{2}\frac{i^k}{k!}n^{(k)}_{2l_{\mathrm{SPM}}}\frac{\partial^k|A_0|^{2l}(t)A_0(t)}{\partial t^k} + \sum_{l=1}^{3}(l+1)!\sum_{k=0}^{3}\frac{i^k}{k!}n^{(k)}_{2l_{\mathrm{XPM}}}\frac{\partial^k|A_0|^{2(l-1)}(t)|A_3|^2(t)A_0(t)}{\partial t^k}\right.$$
$$\left. + \sum_{l=1}^{3}l\sum_{k=0}^{3}\frac{i^k}{k!}n^{(k)}_{2l_{\mathrm{R}_1}}\frac{\partial^k|A_0|^{2(l-1)}A_0^{*2}(t)A_3(t)}{\partial t^k} + \sum_{l=1}^{3}\frac{l(l-1)}{l+2}\sum_{k=0}^{3}\frac{i^k}{k!}n^{(k)}_{2l_{\mathrm{R}_2}}\frac{\partial^k|A_0|^{2(l-2)}A_0^4(t)A_3^*(t)}{\partial t^k}\right), \quad (1)$$

$$\mathcal{P}_{3\omega_0}(t) = 2\sqrt{\frac{2\epsilon_0}{c}}\left(n_{2_{\mathrm{SPM},3\omega_0}}|A_3|^2(t)A_3(t) + 2\sum_{k=0}^{3}\frac{i^k}{k!}n^{(k)}_{2_{\mathrm{XPM}}}\frac{\partial^k|A_0|^2(t)A_3(t)}{\partial t^k} + \sum_{l=1}^{6}\frac{l}{2+l}\sum_{k=0}^{3}\frac{i^k}{k!}n^{(k)}_{2l_{\mathrm{THG}}}\frac{\partial^k|A_0|^{2(l-1)}A_0^3(t)}{\partial t^k}\right), \quad (2)$$

where ϵ_0 is the vacuum permittivity, c is the light velocity in vacuum, A_0 (A_3) is the complex envelope of the fundamental (third-harmonic) field expressed in $\sqrt{\mathrm{W}}/\mathrm{m}$. Equations (1) and (2) are the main results of this work. All the coefficients are summarized in Table I. These equations take into account four distinct mechanisms occurring during the interaction of a field composed by a fundamental and a third-harmonic field and an atom, namely, self-, cross-phase modulation (SPM and XPM), third-harmonic generation (THG), and fission of a third-harmonic photon into three fundamental photons (denoted hereafter recombination [R]). The different mechanisms involved in the nonlinear polarization are summarized in Fig. 1. The equations also take into account the slightly delayed nature of the different processes at play but do not take into account the contribution of ionization to the optical atomic response, which is treated separately. The procedure used to fit the different coefficients is detailed in the next section.

III. WEAK-FIELD FIT PROCEDURE

Each nonlinear effect, namely, SPM, XPM, THG, and recombination (R), can be fitted individually by noting that they do not share the same dependence with respect to the amplitude and phase of the two-color field. It then allows one to minimize the number of free parameters used simultaneously to recover the exact polarization obtained by solving TDSE.

A. Self-phase modulation and third-harmonic generation

Cross-phase modulation and recombination do not occur if there is no third-harmonic or no fundamental field within the initial electric field. In this situation, only SPM and THG take place. Their respective contributions are easily distinguishable since they evolve at very distinct frequencies (close to ω_0 and $3\omega_0$, respectively). After an appropriate spectral filtering, both effects can then be fitted individually as a function of both time and peak intensity.

As shown in Fig. 2, self-phase modulation of the fundamental field is found to behave almost linearly with respect to the intensity up to 20 $\mathrm{TW/cm^2}$. The associated nonlinear refractive index extracted from the fit is $n_{2_{\mathrm{SPM}}} = 2.9\times10^{-7}$ $\mathrm{cm^2/TW}$, in good agreement with data found in the literature [25]. Nevertheless, a closer look at the TDSE results reveals the presence of a positive higher-order Kerr term $n_{4_{\mathrm{SPM}}} = 3.45\times10^{-9}$ $\mathrm{cm^4/TW^2}$. This value agrees also well with data found in the literature [26]. At higher intensity, the polarization saturates and becomes negative in the trailing edge of the field beyond about 50 $\mathrm{TW/cm^2}$. This delayed behavior in the temporal domain is in fact characteristic of the ionization-induced saturation of the atomic optical response.

The nonlinear refractive index relative to the self-phase modulation of the third-harmonic field has been estimated differently. One has to note that two different mechanisms participate to SPM: the one-photon [see Fig. 1(b)] and two-photon [see Fig. 1(c)] contributions. For the third-harmonic

TABLE I. Nonlinear refractive indices of krypton at $\lambda_0 = 400$ nm retrieved from *ab initio* calculations.

k	$n_{2_{SPM},\omega_0}^{(k)}$ (fs^{k}cm^2 TW^{-1})	$n_{4_{SPM}}^{(k)}$ (fs^{k}cm^4 TW^{-2})	$n_{2_R}^{(k)}$ (fs^{k}cm^2 TW^{-1})	$n_{4_{R_1}}^{(k)}$ (fs^{k}cm^4 TW^{-2})
0	$2.92\times10^{-7}-4.88i\times10^{-10}$	$3.45\times10^{-9}+7.27i\times10^{-12}$	$1.82\times10^{-6}-2.37i\times10^{-9}$	$-8.84\times10^{-8}-1.33i\times10^{-9}$
1	2.23×10^{-8}	2.05×10^{-8}	$1.12\times10^{-6}+1.77i\times10^{-8}$	$-2.69\times10^{-8}+1.70i\times10^{-9}$
2	$9.66\times10^{-9}-3.92i\times10^{-9}$	-3.17×10^{-10}	$1.35\times10^{-6}+2.83i\times10^{-7}$	$-7.83\times10^{-8}-3.01i\times10^{-8}$
3	0	0	$-6.07\times10^{-8}-5.67i\times10^{-9}$	$9.52\times10^{-8}+1.26i\times10^{-8}$
k	$n_{4_{R_2}}^{(k)}$ (fs^{k}cm^4 TW^{-2})	$n_{6_{R_1}}^{(k)}$ (fs^{k}cm^6 TW^{-3})	$n_{6_{R_2}}^{(k)}$ (fs^{k}cm^6 TW^{-3})	$n_{2_{XPM}}^{(k)}$ (fs^{k}cm^2 TW^{-1})
0	$-8.91\times10^{-8}-8.99i\times10^{-10}$	$1.14\times10^{-9}+2.48i\times10^{-10}$	$1.09\times10^{-9}+2.14i\times10^{-10}$	$-1.07\times10^{-5}+9.61i\times10^{-7}$
1	$4.81\times10^{-8}+1.77i\times10^{-9}$	$6.81\times10^{-10}-7.26i\times10^{-10}$	$-7.06\times10^{-10}-6.10i\times10^{-10}$	$8.42\times10^{-6}+1.70i\times10^{-6}$
2	$-4.33\times10^{-8}+1.19i\times10^{-8}$	$1.76\times10^{-9}+1.32i\times10^{-9}$	$9.60\times10^{-10}+1.77i\times10^{-11}$	$-4.13\times10^{-6}+8.36i\times10^{-6}$
3	$5.59\times10^{-8}+1.31i\times10^{-9}$	$-3.38\times10^{-9}+2.16i\times10^{-10}$	$1.90\times10^{-10}+1.13i\times10^{-9}$	$2.86\times10^{-6}+1.15i\times10^{-5}$
k	$n_{4_{XPM}}^{(k)}$ (fs^{k}cm^4 TW^{-2})	$n_{6_{XPM}}^{(k)}$ (fs^{k}cm^6 TW^{-3})	$n_{2_{THG}}^{(k)}$ (fs^{k}cm^2 TW^{-1})	$n_{4_{THG}}^{(k)}$ (fs^{k}cm^4 TW^{-2})
0	$1.27\times10^{-7}-4.64i\times10^{-8}$	$1.72\times10^{-9}+1.28i\times10^{-9}$	$1.74\times10^{-6}+2.89i\times10^{-9}$	$-7.80\times10^{-8}+3.54i\times10^{-10}$
1	$-7.35\times10^{-8}-1.74i\times10^{-7}$	$9.51\times10^{-12}+3.10i\times10^{-9}$	$1.41\times10^{-6}-1.00i\times10^{-7}$	$-4.68\times10^{-8}+3.31i\times10^{-8}$
2	$5.69\times10^{-8}-1.51i\times10^{-7}$	$-1.07\times10^{-11}+2.13i\times10^{-9}$	$3.39\times10^{-6}-1.78i\times10^{-7}$	$-1.90\times10^{-7}-1.30i\times10^{-8}$
3	$-1.79\times10^{-7}+5.32i\times10^{-10}$	$9.32\times10^{-10}-7.48i\times10^{-9}$	-1.54×10^{-5}	6.43×10^{-7}
k	$n_{6_{THG}}^{(k)}$ (fs^{k}cm^6 TW^{-3})	$n_{8_{THG}}^{(k)}$ (fs^{k}cm^8 TW^{-4})	$n_{10_{THG}}^{(k)}$ (fs^{k}cm^{10} TW^{-5})	$n_{12_{THG}}^{(k)}$ (fs^{k}cm^{12} TW^{-6})
0	$6.70\times10^{-10}-1.78i\times10^{-10}$	$7.36\times10^{-12}+2.55i\times10^{-11}$	$-1.05\times10^{-13}-4.54i\times10^{-13}$	$2.40\times10^{-16}+2.24i\times10^{-15}$
1	$3.04\times10^{-9}-3.39i\times10^{-9}$	$-1.02\times10^{-10}+8.46i\times10^{-11}$	$1.31\times10^{-12}-8.19i\times10^{-13}$	$-5.61\times10^{-15}+2.81i\times10^{-15}$
2	$7.00\times10^{-9}+3.30i\times10^{-9}$	$-1.16\times10^{-10}-1.21i\times10^{-10}$	$8.25\times10^{-13}+1.51i\times10^{-12}$	$-2.03\times10^{-15}-6.27i\times10^{-15}$
3	-1.03×10^{-8}	-4.73×10^{-14}	1.20×10^{-12}	-6.89×10^{-15}

$$n_{2_{SPM},3\omega_0}(\text{cm}^2\text{TW}^{-1}) = -7.8\times10^{-7}$$

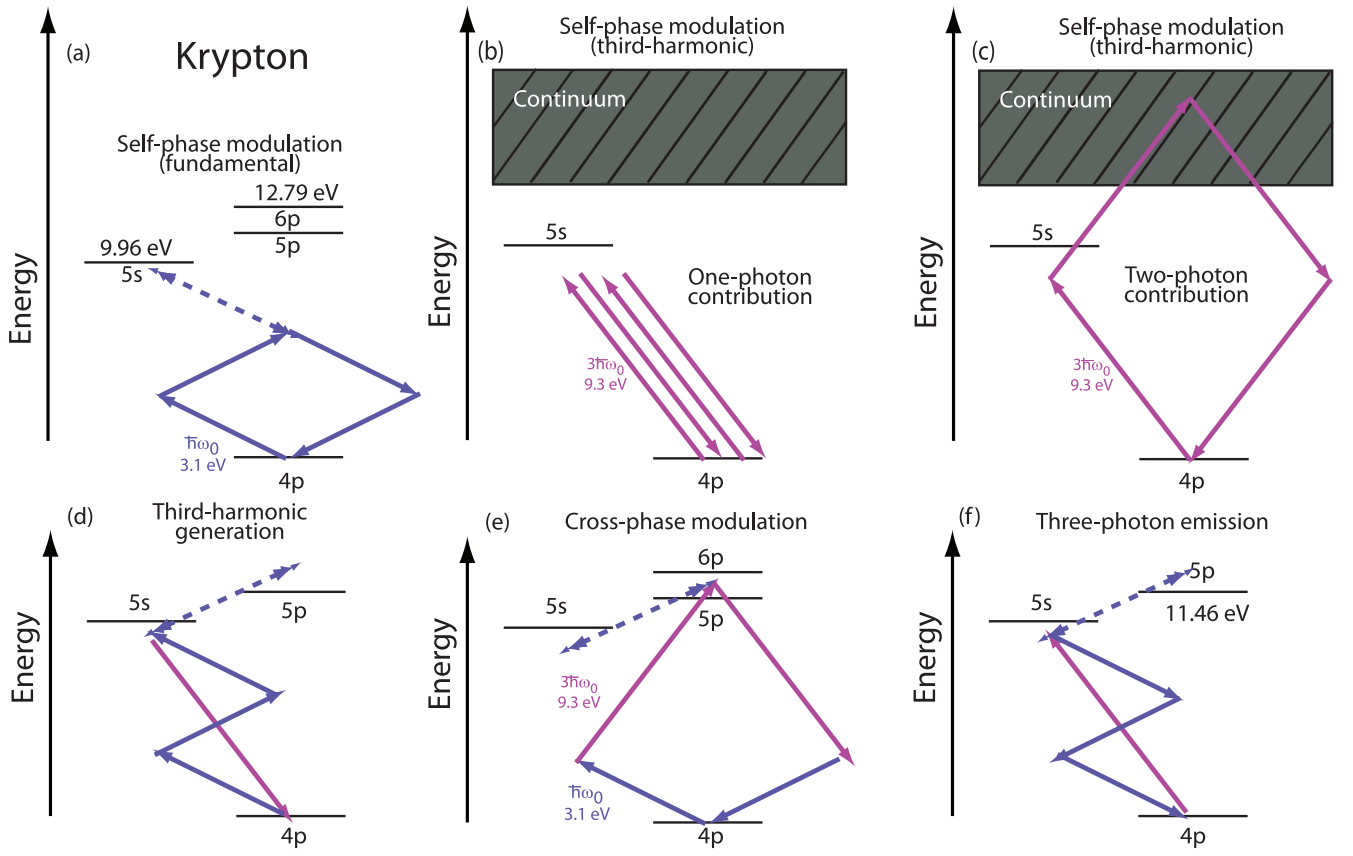

FIG. 1. Nonlinear processes occurring when a krypton atom is irradiated by a fundamental field at 400 nm and its third harmonic: self-phase modulation for the fundamental field (a), one-photon (b), and two-photon (c) contributions to self-phase modulation for the third-harmonic field, third-harmonic generation (d), cross-phase modulation (e), and three-photon emission (f). The dotted arrows stand for higher-order processes enhanced because of resonances.

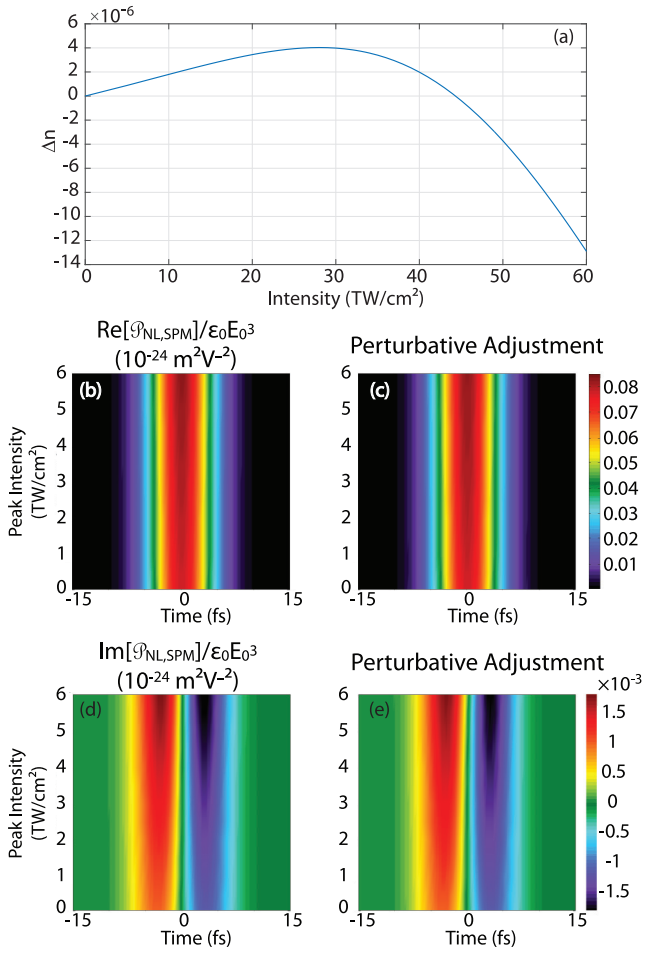

FIG. 2. Nonlinear refractive index of krypton at 400 nm as a function of the pulse intensity (a). Real part of the nonlinear polarization envelope related to self-phase modulation obtained with TDSE (b) and its associated perturbative fit (c). Imaginary part of the nonlinear polarization envelope related to self-phase modulation obtained with TDSE (d) and its associated perturbative fit (e).

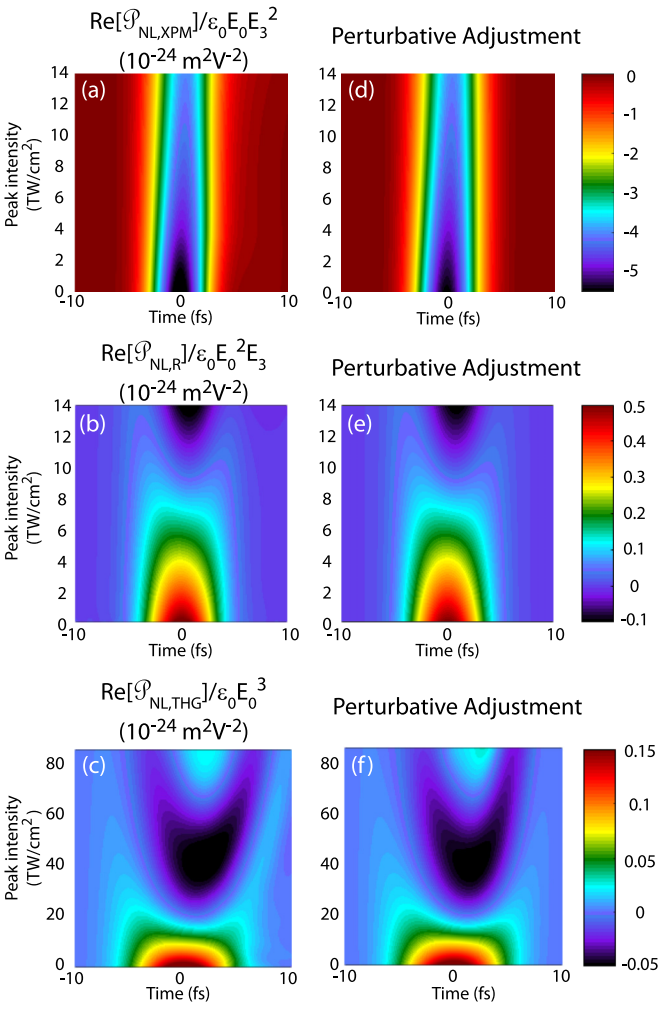

FIG. 3. Contribution of the different processes to the real part of the nonlinear polarization envelope as a function of time and fundamental pulse intensity. Top row: cross-phase modulation induced by a 0.15 TW/cm^2 third-harmonic field calculated by TDSE (a) and the associated higher-order weak-field fit (d). Middle row: recombination induced by a 0.15 TW/cm^2 third-harmonic field calculated by TDSE (b) and the associated higher-order weak-field fit (e). Bottom row: third-harmonic generation (calculated without third-harmonic seed pulse) obtained by solving TDSE (c) and the associated higher-order weak-field fit (f). In order to highlight the impact of HOKE, all the data are normalized to their expected peak field dependence, i.e., the dependence that should follow the nonlinear polarization without higher-order processes.

field ($\lambda_3 \simeq 133$ nm), the two-photon contribution cannot be decoupled from the ionization process in the *ab initio* calculations because the latter is also a two-photon absorption process. This then prevents the identification of the nonlinear refractive index related to SPM of the third-harmonic field from TDSE calculations. In order to circumvent this point, the nonlinear refractive index $n_{2_{\mathrm{SPM}},3\omega_0}$ has been directly evaluated with the dipolar transition moments tabulated from the atomic potential of krypton used in the TDSE and only the one-photon contribution has been retained. This approximation then leads to a negative nonlinear refractive index. Nevertheless, this approximation does not significantly change the conclusion of this work. Indeed, by changing both the value and sign of this index, it has been found that the latter does not play a significant role in the nonlinear propagation dynamics.

In the present case (krypton, $\lambda_0 = 400$ nm), the process of third-harmonic generation also takes place close to a resonance, namely the ($4p$-$5s$) three-photon resonance. As a result, the nonlinear refractive index associated to THG $n_{2_{\mathrm{THG}}}$ is found to be about six times higher than the one associated to SPM. The vicinity of the resonance also impacts both the intensity and the temporal dependencies of the nonlinear polarization. Indeed, far from resonances, it is known that the third-harmonic field amplitude induced by THG behaves as the third power of the fundamental field amplitude. On the contrary, in the present situation, THG does not follow this trend, as it can be seen in Fig. 3(c). Instead, the nonlinear polarization relative to THG $\mathcal{P}_{\mathrm{NL,THG}}$ saturates as the fundamental intensity increases, becomes negative beyond 20 TW/cm^2, and increases again beyond 40 TW/cm^2 up to recovering positive values. This behavior is in fact the manifestation of higher-order nonlinear processes. Note that there is no contribution of ionization to the nonlinear

polarization oscillating at $3\omega_0$ in the case of a fundamental field exciting the atom alone, discarding this effect to be responsible for the observed behavior. More particularly, following a weak-field development, it is found that susceptibilities up to $\chi^{(13)}$ have to be considered for an appropriate fit of the nonlinear polarization associated to THG up to 90 TW/cm^2 [see Fig. 3(f)]. Indeed, not only the process $\omega_0+\omega_0+\omega_0 \rightarrow 3\omega_0$ is close to a resonance but higher-order processes of kind $\omega_0+\omega_0+\omega_0+N(\omega_0-\omega_0) \rightarrow 3\omega_0$ (N being a positive integer) as well. The vicinity of the resonance then exalts higher-order processes.

B. Cross-phase modulation and recombination

Cross-phase modulation and recombination processes contribute to the nonlinear polarization as soon as a fundamental field and its third-harmonic interact together with the atom [see Figs. 1(e) and 1(f)]. Their relative contributions to the nonlinear polarization can be distinguished by noticing that the recombination process depends on the relative phase $\Delta\phi$ between the fields while XPM does not. More particularly, the contribution of recombination to the third-order nonlinear polarization $\mathcal{P}_{\mathrm{R}}(\Delta\phi)$ follows $\mathcal{P}_{\mathrm{R}}(\pi)=-\mathcal{P}_{\mathrm{R}}(0)$. Since this is the only weak-field contribution to the nonlinear polarization that depends on the relative phase, it can be isolated as follows:

$$\mathcal{P}_{\mathrm{R}}=\tfrac{1}{2}(\mathcal{P}_{\mathrm{NL}}(\Delta\phi=0)-\mathcal{P}_{\mathrm{NL}}(\Delta\phi=\pi)), \tag{3}$$

while the contribution of XPM to the nonlinear polarization $\mathcal{P}_{\mathrm{XPM}}$ can be extracted after substraction of the previously evaluated SPM contribution as

$$\mathcal{P}_{\mathrm{XPM}}=\tfrac{1}{2}(\mathcal{P}_{\mathrm{NL}}(\Delta\phi=0)+\mathcal{P}_{\mathrm{NL}}(\Delta\phi=\pi))-\mathcal{P}_{\mathrm{SPM}}. \tag{4}$$

A first set of calculations have been performed at low fundamental intensity ($I_0=1$ TW/cm^2) as a function of the third-harmonic field amplitude. It is found that cross-phase modulation (recombination) well follows the expected linear dependence with respect to the third-harmonic intensity (field amplitude). Moreover, the two processes are almost (but not exactly) instantaneous and approximatively follow their expected temporal dependencies. After fitting the nonlinear polarizations, the associated nonlinear refractive indices are found to be $n_{2_{\mathrm{XPM}}}=-1.07\times10^{-5}$ cm^2/TW and $n_{2_{\mathrm{R}}}=1.82\times10^{-6}$ cm^2/TW, respectively. The first observation is that $n_{2_{\mathrm{XPM}}}$ is negative and about 30 times higher in amplitude than $n_{2_{\mathrm{SPM}}}$. This is because the XPM process takes place at the vicinity of the ($4p$-$5p$) and ($4p$-$6p$) two-photon resonances. The immediate consequence is that while krypton is conventionally a focusing medium for the fundamental field, it becomes defocusing because of XPM if about 1.5% of third-harmonic copropagates together with it. In other words, if enough third-harmonic is generated during the filamentation process in krypton, XPM can be the main physical mechanism arresting the collapse, in place of ionization. Then, XPM and recombination have been evaluated with TDSE as a function of the fundamental intensity, keeping constant the third-harmonic field amplitude. Figures 3(a) and 3(b) show the obtained temporal dependence of $\mathcal{P}_{\mathrm{XPM}}$ and $\mathcal{P}_{\mathrm{R}}$ as a function of the fundamental intensity. Both contributions to the nonlinear polarization do not follow the expected dependence with respect to the fundamental field amplitude. Indeed, far from resonance, the polarization relative to XPM normally behaves as A_0, while those relative to recombination as A_0^2. Here, because of the vicinity of a two-color resonance, higher-order susceptibilities manifest themselves, modifying the dependence with respect to the field amplitude. As far as XPM is concerned, its contribution to the nonlinear polarization has to be expanded at higher order with terms mixing fundamental and third-harmonic intensities. Following a weak-field expansion with respect to the field, two kinds of higher-order terms participate in the recombination process (denoted hereafter R_1 and R_2, respectively). The first (second) kind of higher-order nonlinear polarization $\mathcal{P}_{\mathrm{R}_1}$ ($\mathcal{P}_{\mathrm{R}_2}$) behaves as $|A_0|^{2k}A_0^{*2}A_3$ ($|A_0|^{2k}A_0^4A_3^*$). In the presence of a resonance, their relative contributions are *a priori* different because the frequencies involved in their respective nonlinear susceptibilities are not the same. It is then desirable to fit them independently, which can be done by noting their different periodicity with respect to the relative phase $\Delta\phi$. More particularly, $\mathcal{P}_{\mathrm{R}_1}$ and $\mathcal{P}_{\mathrm{R}_2}$ can be isolated as follows:

$$\begin{aligned}\mathcal{P}_{\mathrm{R}_1}&=\tfrac{1}{2}\{\mathcal{P}_{\mathrm{NL}}(\Delta\phi=0)-\mathcal{P}_{\mathrm{NL}}(\Delta\phi=\pi)\\&\quad-i[\mathcal{P}_{\mathrm{NL}}(\Delta\phi=\pi/2)-\mathcal{P}_{\mathrm{NL}}(\Delta\phi=-\pi/2)]\},\\\mathcal{P}_{\mathrm{R}_2}&=\tfrac{1}{2}\{\mathcal{P}_{\mathrm{NL}}(\Delta\phi=0)-\mathcal{P}_{\mathrm{NL}}(\Delta\phi=\pi)\\&\quad+i[\mathcal{P}_{\mathrm{NL}}(\Delta\phi=\pi/2)-\mathcal{P}_{\mathrm{NL}}(\Delta\phi=-\pi/2)]\}.\end{aligned}$$

C. Noninstantaneous nonlinear processes

Close to a multiphoton resonance, nonlinear susceptibilities become highly frequency dependent. This translates to a noninstantaneous interaction with respect to the exciting field so that the polarization exhibits a delayed component. This is evidenced not only in Fig. 3(c) where the temporal shape of the real part of the nonlinear polarization turns out to be asymmetric (while the exciting field is temporally symmetric), but also by noting that the imaginary part of the nonlinear polarization envelope [see Fig. 4(c)] is in good approximation an odd function of time, at least at low field. The temporal shape of the imaginary component of the nonlinear polarization at low field then indicates that the atomic optical response at $3\omega_0$ is temporally delayed and also that optical losses are very weak. The medium absorbs energy during the rising edge of the pulse and gives it back completely to the field during the falling edge. The energy is then redistributed in time without any net losses. In a mathematical point of view, this can be understood if one expresses the evolution of the intensity I of a field having a complex envelope A as a function of the propagation distance z in a medium that generates a polarization $\mathcal{P}$:

$$\partial_z I(t,z)\propto-\mathrm{Im}[\mathcal{P}(t)A^*(t)]. \tag{5}$$

Since the fluence F of the field reads

$$\int_{-\infty}^{\infty}I(t,z)dt, \tag{6}$$

one obtains the evolution of F along the propagation distance:

$$\partial_z F\propto-\int_{-\infty}^{\infty}\mathrm{Im}[\mathcal{P}(t)A^*(t)]dt. \tag{7}$$

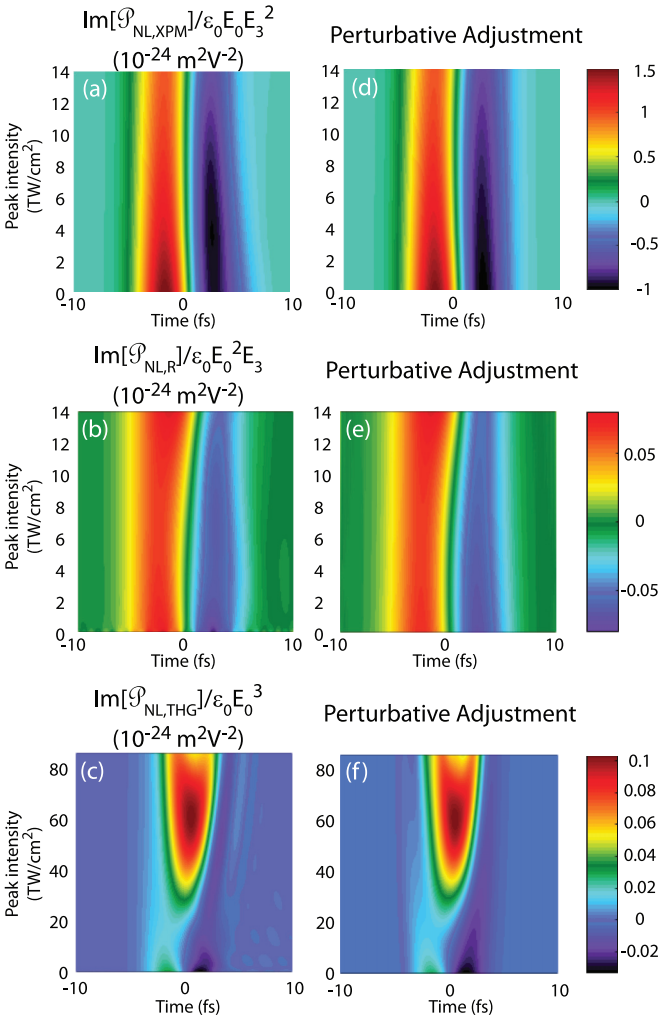

FIG. 4. Contribution of the different processes to the imaginary part of the nonlinear polarization envelope as a function of time and fundamental pulse intensity. Top row: cross-phase modulation induced by a 0.15 TW/cm^2 third-harmonic field calculated by TDSE (a) and the associated higher-order weak-field fit (d). Middle row: recombination induced by a 0.15 TW/cm^2 third-harmonic field calculated by TDSE (b) and the associated higher-order weak-field fit (e). Bottom row: third-harmonic generation (calculated without third-harmonic seed pulse) obtained by solving TDSE (c) and the associated higher-order weak-field fit (f). In order to highlight the impact of HOKE, all the data are normalized to their expected peak field dependence, i.e., the dependence that should follow the nonlinear polarization without higher-order processes.

Without any loss of generality, one can write the function Im($\mathcal{P}$) as the sum of an even and an odd function of time:

$$\mathrm{Im}[\mathcal{P}(t)] = \mathrm{Im}[\mathcal{P}_{\mathrm{odd}}(t)] + \mathrm{Im}[\mathcal{P}_{\mathrm{even}}(t)], \tag{8}$$

with

$$\begin{aligned} \mathrm{Im}[\mathcal{P}_{\mathrm{odd}}(-t)] &= -\mathrm{Im}[\mathcal{P}_{\mathrm{odd}}(t)], \\ \mathrm{Im}[\mathcal{P}_{\mathrm{even}}(-t)] &= \mathrm{Im}[\mathcal{P}_{\mathrm{even}}(t)]. \end{aligned} \tag{9}$$

Since $A(t)$ is an even real function of time in all calculations presented here, one obtains in this case

$$\partial_z F = \int_{-\infty}^{\infty} \mathrm{Im}[\mathcal{P}_{\mathrm{even}}(t)]A(t)dt. \tag{10}$$

As a consequence, only the even part of the polarization induces optical losses.

While the interaction occurs with negligible optical losses at low field, this is not the case anymore as the fundamental field increases. As it can be noticed in Fig. 4(c), for intensities higher than 20 TW/cm^2, the imaginary part of the nonlinear polarization envelope is not an odd function of time anymore. This qualitative change of temporal shape consequently indicates that strong optical losses take place, which is confirmed on the atomic side by the strong increase at high intensity of the populations left in the excited states of the atom after the interaction.

A convenient way to reproduce the temporal shape of the real and imaginary parts of the nonlinear polarization consists in developing the nonlinear susceptibilities as a Taylor development with respect to the frequencies involved in the process. This technique has been already applied in the case where SPM process takes place close to a two-photon resonance [21]. For instance, the third-order nonlinear susceptibility $\chi^{(3)}(\omega_1+\omega_2+\omega_3;\omega_1,\omega_2,\omega_3)$ responsible for THG can be expanded close to $\omega_1+\omega_2+\omega_3 = 3\omega_0$ as

$$\begin{aligned} \chi^{(3)}_{\omega_1,\omega_2,\omega_3} \simeq\ & \chi^{(3)}_{\omega_0,\omega_0,\omega_0} + \sum_{j=1}^{3} \partial_{\omega_j} \chi^{(3)}_{\omega_0,\omega_0,\omega_0}(\omega_j-\omega_0) \\ & + 1/2 \sum_{j=1}^{3} \partial^2_{\omega_j^2} \chi^{(3)}_{\omega_0,\omega_0,\omega_0}(\omega_j-\omega_0)^2 \\ & + \sum_{j\neq k} \partial^2_{\omega_j,\omega_k} \chi^{(3)}_{\omega_0,\omega_0,\omega_0}(\omega_j-\omega_0)(\omega_k-\omega_0) + \cdots . \end{aligned} \tag{11}$$

Supposing that all partial derivatives of the same order are equal, one obtains

$$\chi^{(3)}_{\omega_1,\omega_2,\omega_3} \simeq \sum_k \frac{\chi^{(3)}_k}{k!}(\omega_1+\omega_2+\omega_3-3\omega_0)^k, \tag{12}$$

where $\chi^{(3)}_k = \partial^k_{\omega^k} \chi^{(3)}_{\omega_0,\omega_0,\omega_0}$. Remembering that the nonlinear polarization reads in the frequency domain

$$\begin{aligned} \frac{\widetilde{P}^{(3)}_{\mathrm{NL}}(\omega)}{\epsilon_0} = & \iint \chi^{(3)}_{\omega_1,\omega_2,\omega-(\omega_1+\omega_2)} \widetilde{E}(\omega_1) \\ & \times \widetilde{E}(\omega_2)\widetilde{E}(\omega-(\omega_1+\omega_2))d\omega_1 d\omega_2, \end{aligned} \tag{13}$$

the third-order Taylor expansion of the third-order nonlinear polarization temporal envelope responsible for third-harmonic generation is written as

$$\mathcal{P}^{(3)}_{\mathrm{NL,THG}}(t) = \frac{\epsilon_0}{8} \sum_{k=0} \frac{i^k}{k!} \chi^{(3)}_k \frac{\partial^k \mathcal{A}_0(t)^3}{\partial t^k}, \tag{14}$$

where $\mathcal{A}_0$ is the complex envelope of the fundamental field expressed in V/m. Each term in the development then modifies the temporal shape of the nonlinear polarization in a

different way, the kth Taylor coefficient being responsible for a contribution to the nonlinear polarization, whose temporal shape follows the kth temporal derivative of the process if supposed instantaneous. This difference in the temporal dependence of each terms of the development then facilitates the retrieval of their relative contributions to the polarization. Note that the coefficients $\chi_k^{(3)}$ are *a priori* complex quantities. As it is the case for SPM and THG, XPM, and recombination are not exactly instantaneous. For an appropriate fit result, all processes have been expanded as a Taylor series with respect to the frequency. The perturbative development has been truncated after the third order except for the self-phase modulation term. This is because the latter takes place for frequencies further shifted from resonance than the other terms, as it can be noticed in Fig. 1. As a consequence, the spectral dispersion of the SPM susceptibility is lower (i.e., the process is less delayed in the temporal domain) and a Taylor development to the second order is far sufficient to reproduce the nonlinear polarization related to SPM. The fitted real and imaginary parts of the nonlinear polarizations relative to XPM and recombination are shown in Figs. 3(d), 3(e) and 4(d), 4(e), respectively, and are in excellent agreement with the TDSE results. Finally, note that this mathematical method consisting in developing the nonlinear polarization as a Taylor development with respect to the frequency remains valid as long as the nonlinear polarization behaves smoothly with respect to the frequency, i.e., when the process does not take place at the exact atomic resonance, which is the case in this parametric study. As shown above, this treatment leads to express the nonlinear polarization as a sum of terms proportional to successive temporal derivatives of the field. On the contrary, in the case where the nonlinear polarization oscillates at the exact atomic resonance frequency, a more appropriate treatment would consist in considering the full spectral dependence of the nonlinear susceptibility. It would lead one to express the nonlinear polarization as a convolution between the field and the temporal response of the medium expressed as the Fourier transform of the nonlinear susceptibility.

IV. IMPACT OF THE RESONANCE ON THE FILAMENTATION DYNAMICS

The first question arising after this microscopic study is the impact of the exhibited HOKE on the propagation of a 400 nm pulse in krypton, in particular, in the filamentation regime. As already mentioned above, if only 1.5% of third harmonic is generated during the filamentation process, cross-phase modulation could actively participate and could even become the predominant effect to the intensity clamping of the filament, in place of ionization. In order to elucidate the role of HOKE in the filamentation dynamics, nonlinear propagation simulations have been performed. More particularly, two scenarios have been compared. The first one is the classical scenario of filamentation based on two ingredients: Kerr effect and ionization. The HOKE mechanisms are discarded and the Kerr effect is considered as perfectly instantaneous. As a result, the third-order nonlinear susceptibility becomes frequency independent so that $n_{2_{\mathrm{XPM}}} = n_{2_{\mathrm{R}}} = n_{2_{\mathrm{THG}}} = n_{2_{\mathrm{SPM}}}$. This scenario is compared to the one that takes into account the two-color resonance and its underlying HOKE. Accordingly, the nonlinear polarization can be evaluated in the two different cases and then injected in the unidirectional pulse propagation equation [27] that drives the propagation dynamics of the filament. Both models also embed a phase-dependent two-color ionization rate directly derived from the TDSE results. Both simulations have been conducted in the case of a 500 μJ, 20 fs, and 400 nm pulse with a 1 mm beam radius (FWHM) focused with a 1 m focal lens in 0.1 bar of krypton. Note that the initial pulse duration chosen in this case is longer than the one used for the parametric study performed to fit the different nonlinear refractive indices. It then ensures that the delayed nature of the nonlinear optical response is well reproduced by the Taylor developments of the nonlinear susceptibilities with respect to the frequency, at least at the beginning of the propagation. During the filamentation process, however, it is known that supercontinuum generation leads to a spectral broadening. This could potentially lead to the generation of frequencies potentially resonant with multiphoton atomic transitions, making our model more questionable. In fact, in the filamentation simulations shown below, the spectral broadening of the pulses is sufficiently limited to ensure that the conclusion of our filamentation simulations remains valid.

As shown in Fig. 5, the characteristics of the filament strongly differ depending on the model. The full HOKE model predicts a three times lower intense and two times wider filament than the classical counterpart. On the contrary, the two models predict similar maximal electron density and linear electron density. The difference between the two models is mainly due to two distinct mechanisms. First, the generation of third harmonic is far more efficient in the HOKE model because of the vicinity of the $(4p\text{-}5s)$ three-photon resonance. The impact of the third-harmonic radiation on the fundamental field during the filamentation process is then *de facto* enhanced because more third harmonic is generated. Since the nonlinear refractive index related to XPM is highly negative in the HOKE

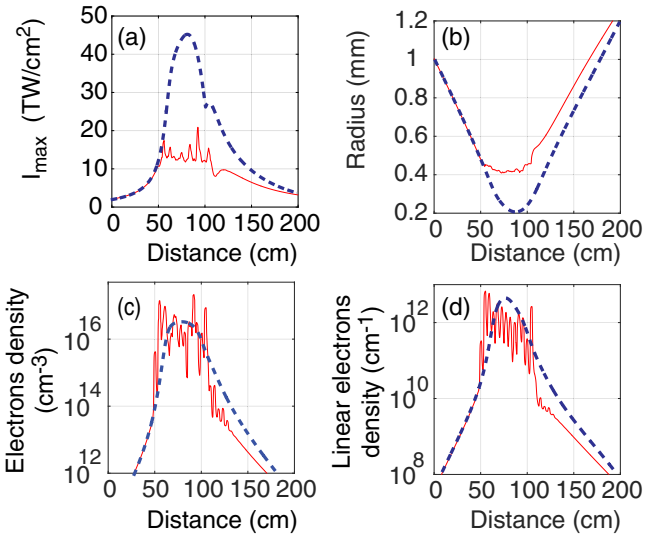

FIG. 5. On-axis intensity (a), FWHM beam radius (b), electrons density (c), and linear density (d) as a function of the propagation distance. The lines in dashed blue (solid red) are obtained with the classical (full HOKE) model.

scenario, the third-harmonic beam defocuses the fundamental one, which lowers the clamping intensity. Secondly, even if the fundamental pulse intensity predicted by the HOKE model is lower, the ionization yield is still comparable to the one predicted by the classical scenario. This is because ionization is greatly enhanced in the presence of third-harmonic radiation. Indeed, as recently demonstrated [17–19], when a fundamental field is accompanied by its third-harmonic, quantum interferences between different ionization channels occur, which results in a very strong enhancement of the ionization rate. As a consequence, ionization still actively participates in the intensity clamping of the filament. Nevertheless, contrary to the usual scenario of filamentation, in which the plasma is the only mechanism that stabilizes the filament, it is found that the defocusing cross-phase modulation induced by the third-harmonic field also plays a major role in the filamentation clamping.

V. CONCLUSION

As a conclusion, the atomic optical response of a gas has been studied in the case where a two-photon transition involving a fundamental field and its third harmonic is close to an atomic resonance. In this situation, the cross-phase modulation, recombination, and third-harmonic generation are strongly enhanced. Moreover, it is shown that higher-order nonlinearities are also strongly boosted and have to be considered for an accurate representation of the nonlinear polarization. Higher-order nonlinear refractive indices have been extracted from TDSE results in the case of krypton for a 400 nm pulse. Finally, the mechanism of filamentation has been studied in this configuration. It is found that the presence of the two-photon resonance strongly modifies the propagation dynamics of the filament as compared to the general case, i.e., far from any resonance. More particularly, it has been shown that the defocusing cross-phase modulation induced by the third-harmonic field on the fundamental one actively participates to the intensity clamping of the filament together with ionization. This highlights the role of the excited bound states in the propagation of ultraviolet filaments. Studied in krypton, the exhibited process should occur in any gas but at different wavelengths (mainly in the UV range) because of the resonant nature of the process. For instance, it is anticipated that a similar trend could occur at 266 nm in argon. Finally, note that the same kind of processes could also take place with higher-order harmonics of visible and near-infrared fields. In particular, giant defocusing cross-phase modulation induced by an odd harmonic as exhibited in the present work can be put in the perspective of the debate concerning the existence of higher-order Kerr effect for 800 nm pulses. Accordingly, one can wonder if the cross-phase modulation induced by higher-order harmonics could have participated in the observations reported in [2].

ACKNOWLEDGMENTS

This work was supported by the Conseil Régional de Bourgogne (PARI program), the CNRS, the French National Research Agency (ANR) through the CoConicS program (Contract No. ANR-13-BS08-0013), and the Labex ACTION program (Contract No. ANR-11-LABX-0001-01). P.B. thanks the CRI-CCUB for CPU loan on its multiprocessor server.

[1] A. Braun, G. Korn, X. Liu, D. Du, J. Squier, and G. Mourou, Opt. Lett. **20**, 73 (1995).
[2] V. Loriot, E. Hertz, B. Lavorel, and O. Faucher, Opt. Express **17**, 13429 (2009).
[3] P. Béjot, J. Kasparian, S. Henin, V. Loriot, T. Vieillard, E. Hertz, O. Faucher, B. Lavorel, and J.-P. Wolf, Phys. Rev. Lett. **104**, 103903 (2010).
[4] P. Béjot, E. Hertz, J. Kasparian, B. Lavorel, J.-P. Wolf, and O. Faucher, Phys. Rev. Lett. **106**, 243902 (2011).
[5] J. K. Wahlstrand and H. M. Milchberg, Opt. Lett. **36**, 3822 (2011).
[6] G. Karras, P. Béjot, J. Houzet, E. Hertz, F. Billard, B. Lavorel, and O. Faucher, Phys. Rev. A **88**, 053424 (2013).
[7] P. Kano, M. Brio, and J. Moloney, Commun. Math. Sci. **4**, 53 (2006).
[8] M. Nurhuda, A. Suda, and K. Midorikawa, Phys. Rev. A **66**, 041802 (2002).
[9] M. Nurhuda, A. Suda, and K. Midorikawa, New J. Phys. **10**, 053006 (2008).
[10] A. Teleki, E. M. Wright, and M. Kolesik, Phys. Rev. A **82**, 065801 (2010).
[11] E. Volkova, A. Popov, and O. Tikhonova, JETP Lett. **94**, 519 (2011).
[12] E. Lorin, S. Chelkowski, E. Zaoui, and A. Bandrauk, Physica D **241**, 1059 (2012).
[13] P. Béjot, E. Cormier, E. Hertz, B. Lavorel, J. Kasparian, J.-P. Wolf, and O. Faucher, Phys. Rev. Lett. **110**, 043902 (2013).
[14] C. Köhler, R. Guichard, E. Lorin, S. Chelkowski, A. D. Bandrauk, L. Berge, and S. Skupin, Phys. Rev. A **87**, 043811 (2013).
[15] C. Brée, A. Demircan, and G. Steinmeyer, Phys. Rev. Lett. **106**, 183902 (2011).
[16] J. K. Wahlstrand, Y. H. Cheng, and H. M. Milchberg, Phys. Rev. Lett. **109**, 113904 (2012).
[17] P. Béjot, G. Karras, F. Billard, E. Hertz, B. Lavorel, E. Cormier, and O. Faucher, Phys. Rev. Lett. **112**, 203902 (2014).
[18] P. Béjot, G. Karras, F. Billard, J. Doussot, E. Hertz, B. Lavorel, and O. Faucher, Phys. Rev. A **92**, 053417 (2015).
[19] J. Doussot, P. Béjot, G. Karras, F. Billard, and O. Faucher, J. Phys. B **48**, 184005 (2015).
[20] J. Doussot, P. Béjot, and O. Faucher, Phys. Rev. A **93**, 033857 (2016).
[21] C. Köhler, L. Bergé, and S. Skupin, Physica D **240**, 963 (2011).
[22] H. Bachau, E. Cormier, P. Decleva, J. E. Hansen, and F. Martin, Rep. Prog. Phys. **64**, 1815 (2001).
[23] F. Cloux, B. Fabre, and B. Pons, Phys. Rev. A **91**, 023415 (2015).
[24] V. V. Strelkov, Phys. Rev. A **93**, 053812 (2016).
[25] C. Brée, A. Demircan, and G. Steinmeyer, IEEE J. Quantum Electron. **46**, 433 (2010).
[26] M. Tarazkar, D. A. Romanov, and R. J. Levis, Phys. Rev. A **90**, 062514 (2014).
[27] M. Kolesik and J. V. Moloney, Phys. Rev. E **70**, 036604 (2004).